



Effect of Ag doping on bipolar switching operation in molybdenum trioxide (MoO_3) nanostructures for non-volatile memory

Mohanbabu Bharathi^{a,d}, Babu Balraj^b, Chandrasekar Sivakumar^b, Zhiwei Wang^{a,d}, Jianwei Shuai^c, Mon-Shu Ho^b, Donghui Guo^{a,d,*}

^a National Model Institute of Microelectronics, Xiamen University, Xiamen 361005, China

^b Department of Physics, National Chung Hsing University, University, Taichung City 402, Taiwan, ROC

^c Department of Physics, Xiamen University, Xiamen 361005, China

^d IC Design R&D Center of Fujian Province, Xiamen University, 361005, China



ARTICLE INFO

Article history:

Received 15 September 2020

Received in revised form 1 November 2020

Accepted 18 November 2020

Available online 23 November 2020

Keywords:

Memristor

Conduction mechanism

Space-charge limited conduction

Doping effect

ReRAM

ABSTRACT

As an emerging technology, nanoscale non-volatile memory technology can be used for in-memory computing and neuromorphic computing. However, the deeper understanding of the charge transport and resistive switching mechanism in memristor devices are still needed to improve the device properties for practical application. Herein, we first synthesized the MoO_3 nanorods and studied the structural properties by XRD, SEM and TEM. The elemental compositions were confirmed through EDX and XPS analysis. The resistive switching operation of Au/ MoO_3 /p-Si ReRAM device was examined and its conductive mechanism was analyzed by space-charge limited conduction theory. The changes of high resistive state to low resistive state and vice-versa in ReRAM device is owing to the movement of oxygen vacancies in MoO_3 structure. For comparison, silver atoms were intercalated into MoO_3 Nanostructures and device performance was also analyzed. The improved switching behavior of Ag doped Au/ MoO_3 /p-Si device is due to Ag doping effect in the formation of conducting paths in the MoO_3 active material. The obtained results indicate the contribution of Ag atoms in conduction filament enhance the bipolar resistive switching performance.

© 2020 Elsevier B.V. All rights reserved.

1. Introduction

Recently, a large amount of data is generated because of rapid development in the information technologies. In this big data era, a revolution is required in the development of new materials and devices for future industries, as current manufacturing unit is reaching their physical limits [1,2]. Emerging nanoscale non-volatile memory technology is one of the key solutions for next generation technologies. Since the first proposal of memristor concept [3] and implementation of memristor device [4], enormous research works have been reported in the field of nanoscale memristor devices as perceived in many review articles [5–9]. Such attention has been given due to its potential properties like excellent endurance, retention, and non-volatility [10,11] to replace conventional memory devices [12]. In addition, nanoscale memristor devices are also highly demanded for applications in bio-inspired neuromorphic

computing [13,14]. Such devices play a key role in manipulating advanced technologies beyond Moor's law and von Neumann bottleneck [15,16]. At present, one of the foremost hindrances for resistive switching memory development and application is the indetermination of physical conductive charge transport property and tunability resistive switching in nanoscale devices. Consequently, memristors are still need to be studied in depth.

In order to comprehend and improve the consistency of memristor devices, a good number of resistive active materials including oxide-based nanomaterials like WO_3 [17], TiO_x [18], ZnO [19], HfO_2 [20] and etc., has been studied in recent years. As such, molybdenum trioxide (MoO_3), is a potential transition metal oxide, promise for use as active nanomaterial for resistive switching devices because of thermodynamic stability, high reactivity and wider band gap [21, 22]. In addition, the property of low carrier concentration in MoO_3 nanomaterials could find potential applications as active material to avoid extra current and energy consumption in memristor devices. Recently, Dai et al., proposed a MoO_{3-x} based memristor device to realize the consistent resistive switching parameters [23]. The movement of positively charged oxygen vacancies makes this layer more conductive and enable typical bipolar resistive switching

Abbreviations: MoO_3 , Molybdenum trioxide; Ag, Silver; Au, Gold; p-Si, P-type Silicon; ReRAM, Resistive random-access memory; SCLC, space charge limited current

* Corresponding author.

E-mail address: dhguo@xmu.edu.cn (D. Guo).

property. It has been extensively accepted the migration of oxygen vacancies form conductive path for charge transport in resistive switching devices [24]. Arita et al., investigated the resistive switching properties of MoO_3 thin films [25,26].

The typical concern about uniformity and tunability of resistive switching in nanoscale devices could be resolved by effective doping method. The electrical uniformity has been achieved by doping method in previously reported work [27,28]. The role of oxygen vacancies in forming conduction path plays a major role in most of the scientific works on memristor devices. Nonetheless, the effect of dopant has been given less emphasize in resistive switching. Some of works disclose the doped system could be possible solution for achieving efficient device performance. The performance of the device has been improved with introduction of metal nanoparticles in active layer by Goswami et al., [29]. Likewise, Lei Wu et al. introduced the Al metal in active dielectric layer to demonstrate the multilevel resistance state in the nanoscale memristor device [30]. The bio-synapse based on Ca^{2+} or Na^+ ions can be emulated by diffusion of doped Ag atom in oxide based active materials [31]. Hence, the electrochemically active materials can be conveniently doped with MoO_3 nano materials to manipulate ion intercalation in the structure.

In this work, the significance of the electrochemically active metal silver (Ag) atom doped in MoO_3 nanostructure has been analyzed for memristor applications. The carrier concentration in the ReRAM device is tuned by adding silver atom with MoO_3 nanostructure. The solution processed pure and Ag doped MoO_3 ReRAM devices have been fabricated and analyzed its resistive switching parameters for better understanding of conduction mechanism in device. The fabricated $\text{Au}/\text{MoO}_3/\text{p-Si}$ and $\text{Au}/\text{Ag}/\text{MoO}_3/\text{p-Si}$ memory devices showed typical bipolar switching property. In addition, the performance of the MoO_3 device enhanced by Ag dopant is also reported in this letter.

2. Experimental section

2.1. Preparation of pure and Ag doped MoO_3 nanoparticles

The synthesis of pure MoO_3 and Ag-doped MoO_3 nanoparticles is done by a wet chemical route. Analytical grade chemicals of ammonium heptamolybdate tetrahydrate (AHMT), sodium dodecyl sulfate (SDS), ethanol and silver nitrate (AgNO_3) are used as purchased without any further purification in this preparation process. The synthesis process furnished in following steps.

Step I: AHMT is taken according to the required amount and dissolved in distilled water to result a concentration of 0.2 M with the support of magnetic stirrer for 30 min. The pale white color precipitate is formed after adding the concentrated solution of SDS, generally used as surfactant. The mixture is constantly stirred for approximately 30 min until a white precipitate is formed. Subsequently, the ethanol solution is added drop wise in the mixture to get a pure white precipitate which later turns into colloidal phase. This colloidal solution is dried on a hot plate for 24 h until the solid sample is formed.

After the reaction hour, the solid yields are obtained by filtering. Further, the yields are purified by the centrifugation (2000 rpm/15 min) several times with distilled water and ethanol separately. The purified yields are dried in an oven at 150 °C for 5 h. Afterwards, the dried sample is calcinated at 400 °C for 3 h. Then, the system is allowed to cool down to room temperature at rate of 5 °C/min. Finally, the prepared white sample turned into pale blue MoO_3 nanoparticles. The obtained MoO_3 nanoparticles are used for further studies.

Step II: For the synthesis of Ag-doped MoO_3 , silver nitrate is used as dopant precursor solution. An estimated amount of silver nitrate is mixed with aqueous Ammonium heptamolybdate tetrahydrate

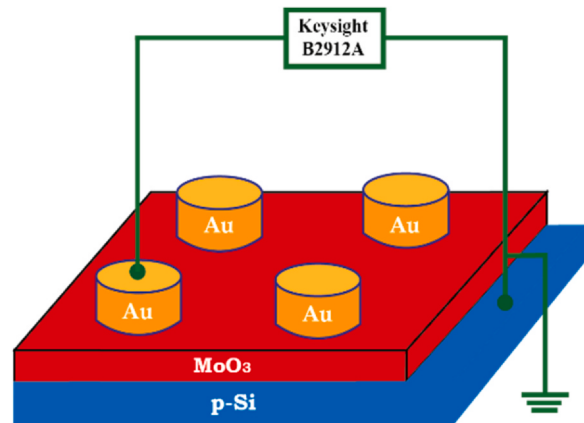


Fig. 1. Schematic representation of device structure.

solution for preparation of various concentration of silver atom (5 wt % and 10 wt%) in MoO_3 nanoparticles. In addition, a required amount of SDS is also added into the homogenous mixture in drop wise. The same Step I procedure is followed to obtain the Ag (5 wt% and 10 wt %) doped MoO_3 nanoparticles. The prepared Ag doped MoO_3 nanoparticles are used for fabrication for devices.

2.2. Device fabrication

The synthesized pure and Ag doped MoO_3 nanomaterials are used to fabricate the ReRAM devices. The synthesized nanomaterials are dispersed in xylene and the solution is used in spin coating technique to deposit MoO_3 . The n-type Si (100) with size of 1 cm² is used as bottom electrode for fabricating devices. The three-step spin coating procedure has been followed to deposit pure and Ag doped MoO_3 on n-Si substrate. The thermal evaporation method was used to deposit Au top electrode at base pressure of 2.0×10^{-6} Torr. The circular pattern of top electrode is formed by a shadow mask. The patterned Au top electrode is obtained with size of 100 μm diameter and 50 nm thickness. Thus, ReRAM devices has been developed with a total of 100 memory cells of Au top electrode pattern. In this way, pure MoO_3 (Device A), Ag (5 wt%) doped MoO_3 (Device B), and Ag (10 wt%) doped MoO_3 (Device C) have been fabricated as shown in Fig. 1 and examined their resistance switching behavior for memristor applications.

2.3. Characterization technique

The electrical characterization of the fabricated devices is performed in ambient atmosphere by Keysight B2912A Precision Source and Measure Unit. The electrical measurements were calculated by applying voltage bias on the Au top electrodes as well the bottom electrode was grounded. JEOL JSM-7800F Prime Schottky Field Emission Scanning Electron Microscope was used to analysis the morphology of the synthesized nanostructured of MoO_3 . The High-resolution transmission electron microscopy images and selected area electron diffraction patterns of the MoO_3 nanostructures were obtained by JEOL JEM-2100F HRTEM. The crystalline nature and structure of the active layer were characterized using a PANalytical X'Pert Pro MRD X-ray diffractometer. The crystallite size of the pure and Ag doped MoO_3 nanostructures were calculated by Debye-Scherrer formula with the help of measured XRD peak data.

2.4. Memristor theory

Memristor is considered as one of the basic circuit elements along with resistor, capacitor and inductor. The missing relationship

between the charge and the flux was compensated by the discovery of the memristor [3], which is expressed in equation below,

$$d\phi = M(q) dq \quad (1)$$

Where, $M(q)$ represents the memristor function. Dividing both sides by dt , we get

$$V = M(q) i \quad (2)$$

The Eq. (2) represents the ohms linear equation for resistor, when $M(q)$ is constant. However, $M(q)$ is nonlinear element rather than constant in the memristor device equation. Though the Eq. (2) is similar to resistor equation, memristor element $M(q)$ remembers the previous resistance state. HP scientist have realized the memristor device in 2008 [4]. The HP memristor is realized by sandwich titanium dioxide layer between two platinum electrodes. The oxygen vacancies available in the active layer alter the conductance of the device. When electric field is applied, the oxygen breakdown from the metal oxide and make space charge region which rise the conductivity. This is due to drifting the charge carriers in the active layer. The space charge region is not altered by without applying external electric field. The conductance modulation can be expressed by the following memresistance equation.

$$M(x) = R_{LRS}x + R_{HRS}(1 - x), \text{ where } 0 \leq x \leq 1, \quad (3)$$

The x represents the space charge region in device, RLRS represents resistance of high conductance state and RHRS represents resistance of low conductance state of device. The variable space charge region x depends on the mobility of the charge carrier (oxygen vacancies), current flowing through device and thickness of the active layer. Hence, the state equation can be expressed as,

$$\frac{dx}{dt} = \frac{\mu R}{D} i(t) \quad (4)$$

Thus, the device holds both resistor and memory property. As the memresistance of device is function of space charge carrier (oxygen vacancies), the inserted additional charge carrier might have increased the conductance of the memristor device. Hence, the dopant Ag atoms have been inserted in the MoO_3 active layer of the device and the performance of the device has been improved by increased space charge carriers.

2.5. Description of the oxygen exchange mechanism

As any other metal oxides, MoO_3 exhibits nonstoichiometric structure and a lattice disorder at ambient temperature. In addition, the bonds between oxygen and Molybdenum metal breaks under applied electric field, and thus oxygen anions and metal cations are formed. When oxygen ion leaves the lattice site, the oxygen vacancies are created in the MoO_3 resistance switching material. oxygen vacancies are positively charged, and hence act as donor centers. These oxygen vacancies are much more mobile and may lead to an ionic conductivity even at room temperature. According to Kroger and Vink notation [32], the oxygen ion and vacancy creation is taking place by following reaction equation.

$$O \Leftrightarrow \frac{1}{2}O_2(g) + V_O + 2e \quad (5)$$

where oxygen ions in the lattice sites and oxygen vacancies are represented as O_O and V_O , respectively. The transition metal (Mo) ions in the oxide is reduced to a lower valence state, and subsequently oxidized back to stable stoichiometric MoO_3 molecular composite. Both redox process and oxygen migration causes the creation and destruction of conductive path inside active oxide materials between two electrodes. The proposed chemical reaction between Mo ions and oxygen ions are represented in the following equation.

$$\text{MoO}_3 \Leftrightarrow \text{Mo}_{\text{Mo}}^x(\text{MoO}_3) + V_O + O_i \quad (6)$$

The MoO_3 crystal lattice possesses significant point defects which include the vacancies in all sublattices of electrons, holes, and substitutional impurities. Further, the defects in the crystal structure can substantially modified by doping other metal atoms. If the doped impurities have lesser charge than the Mo cation, they act as acceptors A. They act as donors D in case of higher charges.

$$A \Leftrightarrow A^- + h \quad (7)$$

$$D \Leftrightarrow D^+ + e \quad (8)$$

$$\emptyset \Leftrightarrow e + h \quad (9)$$

Where h represents hole and e represents electron and \emptyset represents ground state of any bands in electronic structure. These equations highlight the Impurities ionization process in the crystal structure. These defects create a short circuit in the insulating active MoO_3 nanostructures between electrodes. And thus, the resistance of the switching layer is modified by drifting the defects in the nanostructures. This kind of nanowires created inside the dielectric material will play a significant role in designing ReRAM devices. The rate of concentration changes in oxygen vacancies is very less to significantly alter the conductivity at low voltage. But when voltage reaches a particular high value, the ions creation and migration will not obey the linear transportation theory. Hence, the space charge limited current theory has been proposed in our device to understand more about switching mechanism.

3. Result and discussion

3.1. XRD

The synthesized pure and Ag doped MoO_3 nanostructures are subjected to XRD analysis to determine the phase and crystallinity of the material. The obtained XRD patterns for pure and Ag (5 wt% and 10 wt%) doped MoO_3 are depicted in Fig. 2. The observed diffraction peaks are obviously corresponding the peaks of pure MoO_3 in previously reported nanoparticle work [33]. The peaks at 2θ values of 12.65° , 23.16° , 25.52° , 27.15° , 33.53° , 39.01° , 44.64° and 49.18° are assigned to the monoclinic MoO_3 (JCPDF - no.47-1320). The highest peak observed at 27.15° is attributed to the diffraction from (011) plane of MoO_3 . the high crystallinity of the synthesized nanostructures is identified by the occurrence of sharp diffraction peaks in the spectrum. The absence of any other diffraction peaks indicates the purity of the MoO_3 . For the XRD of Ag-doped MoO_3 (Fig. 2), the intensity peak at 38.13° is agree with (111) of silver XRD data

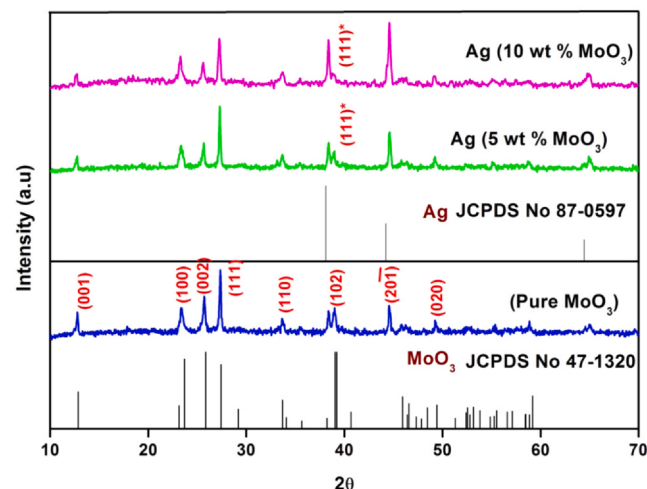


Fig. 2. XRD comparison spectra of pure and Ag doped MoO_3 nanorods.

(JCPDF - no.87-0597). The purity of the Ag doped MoO_3 is appraised with detection of no other peaks. Correspondingly, this is also attributed to the even spreading of doped silver atoms in the MoO_3 nanostructures. It was also noticed from the Fig. 2 that the increase of Ag content in the MoO_3 nanostructure amplified the peak intensity corresponding to Ag (111) plan. The observed changes in XRD spectrum confirms the presence of doped Ag atoms in MoO_3 nanostructure. In addition, the incorporation of higher radius Ag atom in the MoO_3 crystal lattice shows lattice distortion in the crystal structure. Usually, the Debye-Scherrer formula has been used to calculate the crystallite size.

$$\text{Debye - Scherer formula, crystallite size } D = \frac{k\lambda}{\beta_{hkl} \cos\theta} \quad (10)$$

where k represents shape factor (0.9), λ represents wavelength of the radiation, β_{hkl} integral breadth of the reflection, and θ represents angle of reflection. The calculated crystallite size of the pure and doped MoO_3 nanostructures are 48.31 nm and 68.14 nm, respectively. The calculated results confirm the dopant Ag atom modified the crystallite size of the MoO_3 nanostructure. Thus, the XRD spectrum suggested the dopant Ag atom influenced the structural properties of the MoO_3 nanomaterial and accordingly alter the electrical property for memristor application.

3.2. Surface morphology

The surface morphology of the pure MoO_3 and Ag doped MoO_3 nanomaterials was analyzed by SEM and shown in Fig. 3. For pure MoO_3 material, a unique nanorod shaped morphology with smooth surface was observed. The nanorods morphology changes into small nanosheets by doping Ag (5 wt%) atoms with MoO_3 (Fig. 3c). The inclusion of higher atomic radius Ag atoms in the MoO_3 lattice to replace Mo ions leads to the distortion of the lattice. As a result, the

higher concentration of Ag facilitated the growth of primary grains during nucleation and thus contributed to the development of a sheet structure [34]. The morphology of the material become less smooth surface as doped Ag atoms increased to 10 wt percentage. The morphology of Ag (10 wt%) doped MoO_3 is depicted in Fig. 3d. The morphology of the MoO_3 nanorods is also studied examined by TEM analysis. The TEM images of the nanorods are depicted in the Fig. 4(a and d). The HRTEM image of pure and Ag (10 wt%) doped MoO_3 nanorods are shown in Fig. 4b and 4e. The HRTEM image of (4b) shows the presence of mono-crystalline MoO_3 nanorods. It confirms the synthesis of monocrystalline MoO_3 and corroborated with the results of corresponding XRD and SAED patterns. The HRTEM image of (4e) also shows monocrystalline structure but with little distortion in the crystal structure. Correspondingly, the selected area electron diffraction pattern of the synthesized nanomaterials has also been reported in the Fig. 4c and 4f.

3.3. Elemental composition analysis

The quantitative and qualitative analysis of the pure and Ag-doped MoO_3 was carried out on the basis of EDS spectra and the elemental composition. The EDAX spectra of pure and Ag-doped MoO_3 with different concentrations are shown in Fig. 5. The elemental composition of pure and Ag-doped MoO_3 samples are listed in the Table 1. The Mo and O peaks can be obviously found in the spectra but lack of any other peaks in Fig. 5a indicates that the sample is composed of pure MoO_3 nanoparticles. Fig. 5b and 5c show the different ratio of silver doped MoO_3 nanostructure. It was found that the intensity of Ag peak increased with the increase in silver atom concentration. XPS is used to analyze changes in component chemical state (Fig. 6(a-d)). Fig. 6(a) shows the spectrum of survey scans, which consists of peaks of Mo 3d and O1 at their identified positions. The XPS peak of Ag 3d and change in the O1s spectrum proves the existence of Ag in the MoO_3 . Also, the EDAX analysis

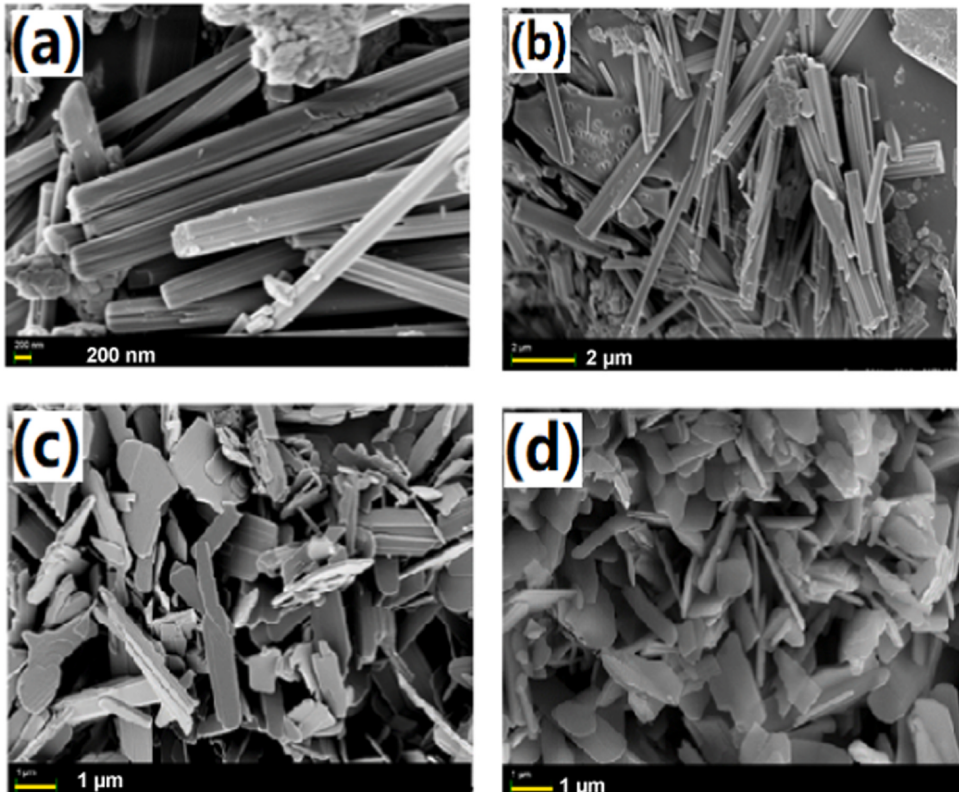


Fig. 3. (a-d) SEM morphology (a-b) pure MoO_3 (c) 5 wt% of Ag doped MoO_3 (d) 10 wt% of Ag doped MoO_3 nanorods.

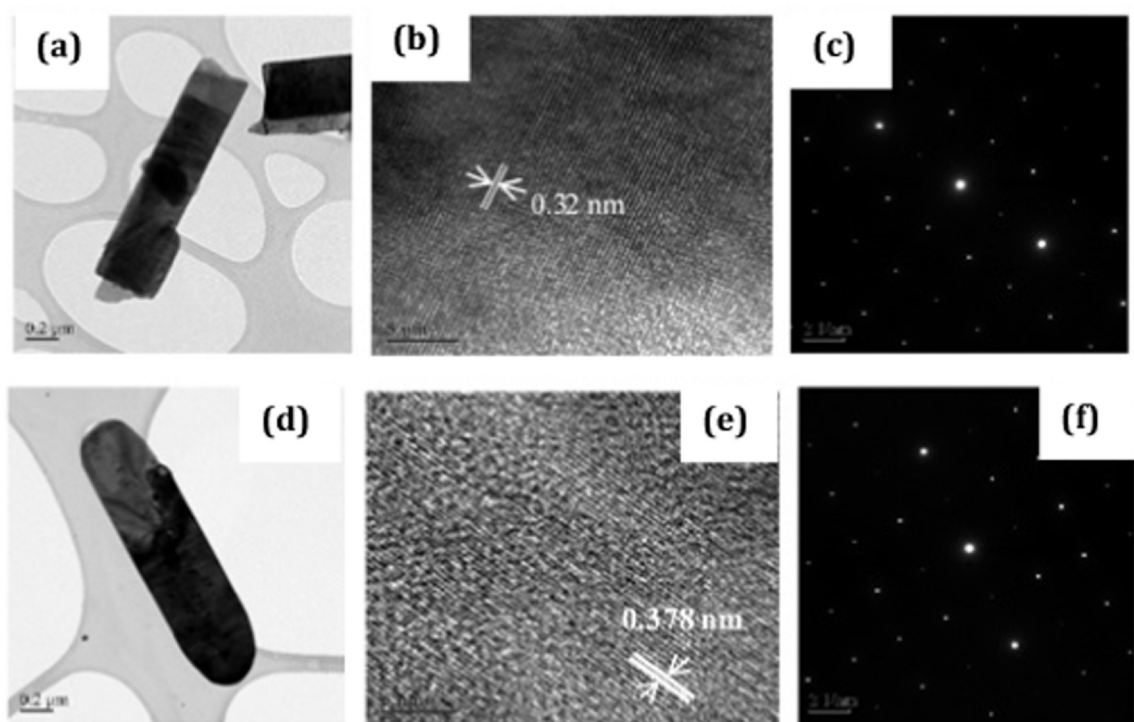


Fig. 4. TEM images of pure and Ag doped MoO_3 nanorods: (a) morphology of pure MoO_3 (b) high resolution image of pure MoO_3 (c) lattice diffraction of pure MoO_3 (d) morphology of Ag: MoO_3 (e) high resolution image of Ag: MoO_3 (f) lattice diffraction of Ag: MoO_3 .

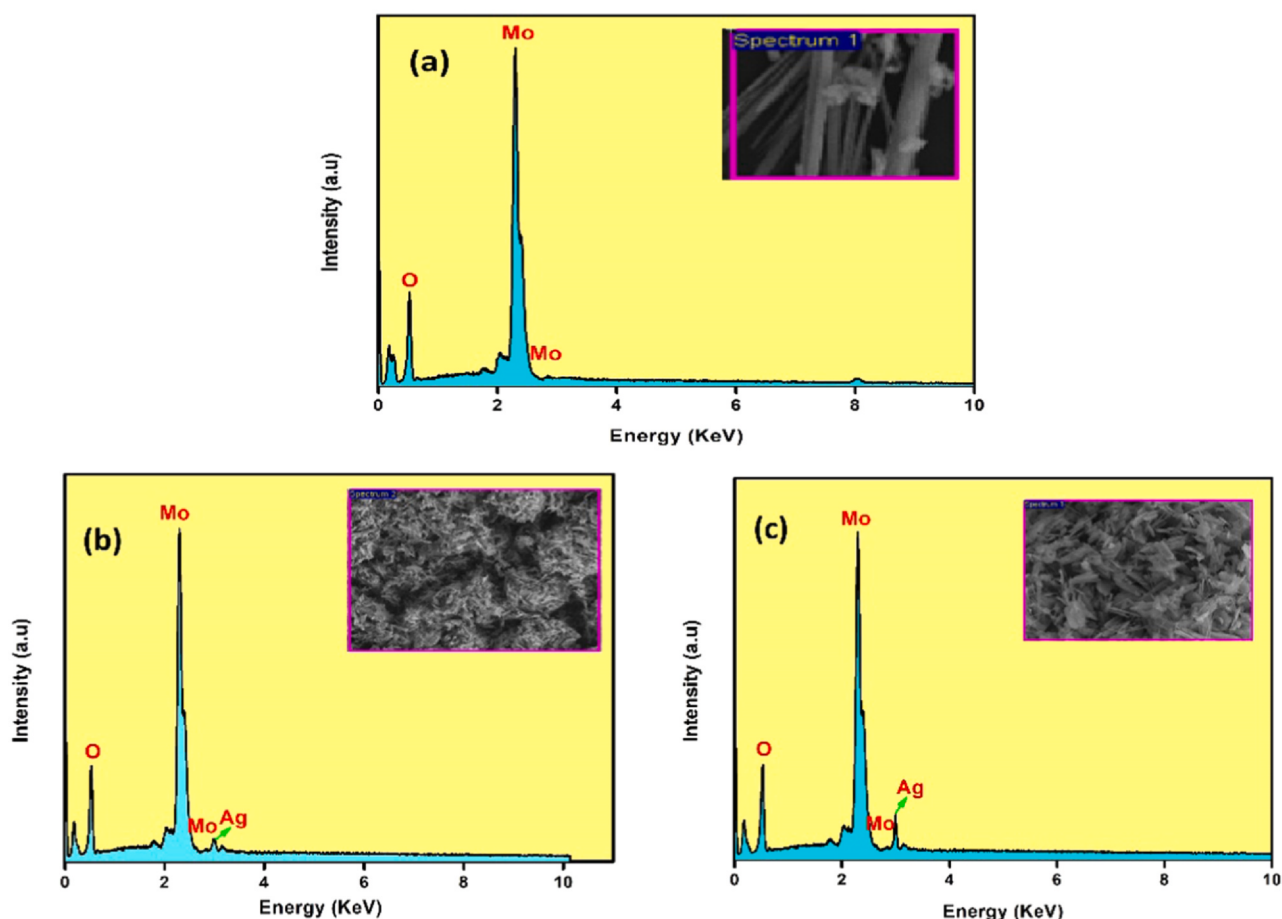


Fig. 5. EDAX spectra of pure and Ag doped MoO_3 nanorods: (a) pure MoO_3 (b) 5 wt% of Ag doped MoO_3 (c) 10 wt% of Ag doped MoO_3 .

Table 1

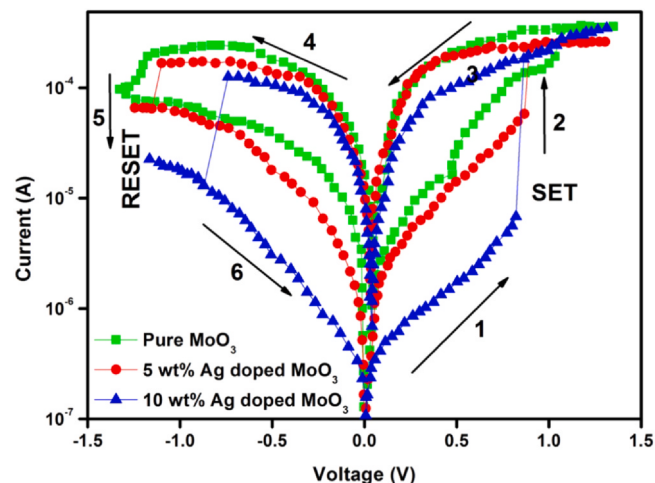
Elemental composition in the nanostructure.

Element	Pure		5 wt%		10 wt%	
	Weight%	Atomic%	Weight%	Atomic%	Weight%	Atomic%
O	41.49	80.96	29.05	71.22	29.15	71.49
Mo	58.51	19.04	66.05	27.00	60.50	24.74
Ag	–	–	4.90	1.78	10.35	3.77

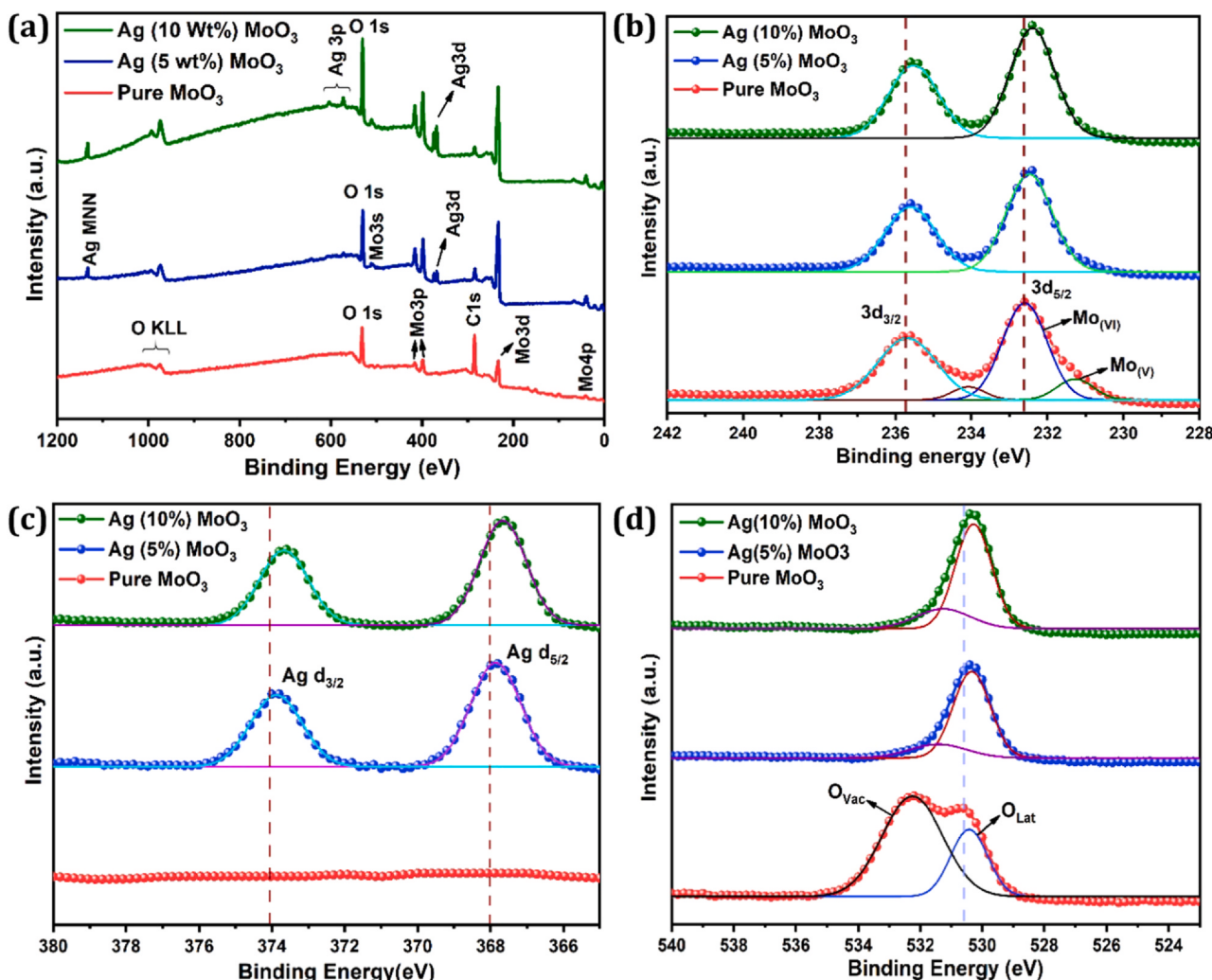
supports the XPS peaks of materials in the samples. In MoO_3 the Mo $3d_{3/2}$ and Mo $5d_{5/2}$ core level range is dominated by double spin orbit peaks, with binding energies of 232.35 and 235.73 eV. The peaks at Ag 368 and 374 eV were attributed to the Ag $3d_{3/2}$ and Ag $5d_{5/2}$ [35].

3.4. ReRAM

To investigate the memory device switching behaviors of the pure MoO_3 and Ag doped MoO_3 ReRAM units, the direct current electrical bias was applied on the Au top electrode (TE), while p-Si bottom electrode (BE) was grounded. The typical current voltage (IV) characteristic of fabricated Au/ MoO_3 /p-Si and Au/Ag: MoO_3 /p-Si devices is depicted in Fig. 7. The initial forming process of switching from high resistance phase into low resistance phase was observed in device A, when a large positive voltage is applied about 2 V. In order to prevent the permanent dielectric breakdown of the device,

Fig. 7. Resistive switching performance of MoO_3 devices.

the low resistive state current is limited by a compliance current of 1 mA during repeatable voltage sweeping ($0 \text{ V} \rightarrow +2 \text{ V} \rightarrow 0 \text{ V} \rightarrow -2 \text{ V} \rightarrow 0 \text{ V}$). Afterwards, when a positive voltage bias is applied, the relative amount of current increases suddenly at 1.1 V. It is because the device resistance changes from high resistance state (HRS) to low resistance state (LRS), which is defined as SET process. The oxygen

Fig. 6. XPS spectra obtained for pure and Ag doped MoO_3 samples (a) Survey scan spectra, (b) Mo 3d core scan spectra (c) Ag 3d core scan spectra and (d) O1s core scan spectra.

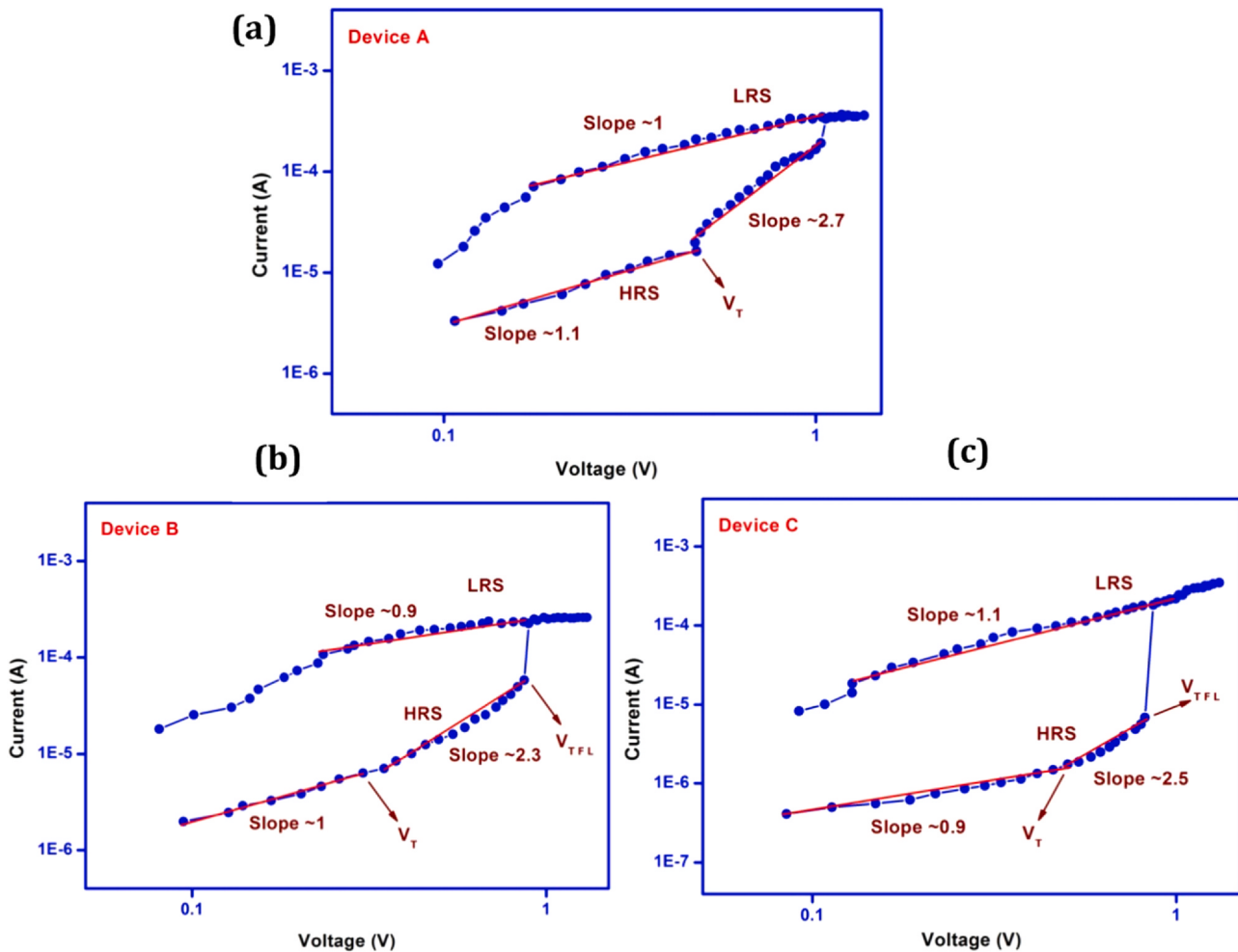


Fig. 8. (a-c) I-V curve analysis for SCLC mechanism of devices: (a) pure MoO_3 (b) 5 wt% of Ag doped MoO_3 (c) 10 wt% of Ag doped MoO_3 nanorods.

vacancies in the device is redistributed when the applied electric field strength reaches the threshold value (1.1 V). It causes the formation of localized metal paths bridging the top and bottom electrodes, thereby increasing current is observed in the device [36]. The device remained in the LRS for subsequently descending voltage, and the LRS was progressively changed to the HRS only by a voltage sweep in the negative voltage region (0 V \rightarrow -2 V). Thus, RESET process was observed in the device at \sim 1.3 V. these SET and RESET processes are repeated for consecutive cycles under positive and negative voltage sweeps. Therefore, the $\text{Au}/\text{MoO}_3/\text{p-Si}$ device exhibits bipolar resistive switching behavior.

The bipolar resistive switching behavior of Ag doped MoO_3 devices are also studied. Both 5 wt% and 10 wt% Ag doped MoO_3 devices discloses the same kind of bipolar resistive switching processes under consecutive voltage cycles. The Fig. 7 shows the bipolar resistive switching behavior of $\text{Au}/\text{Pure MoO}_3/\text{p-Si}$ and Au/Ag (5 wt% and 10 wt%) doped $\text{MoO}_3/\text{p-Si}$ RRAM devices. The SET process was observed at \sim 0.8 V for Ag doped devices while pure MoO_3 device shows the SET process at \sim 1.1 V. Correspondingly, the switching ratio is also increased by adding the Ag in the device. In 0.05% Ag doped MoO_3 device, The switching current changes from 56 micro A at HRS to 241 μA at LRS. similarly, 0.1% Ag doped MoO_3 device shows the switching current from 6 μA to 187 μA during positive voltage sweep. This device has a better switching performance than the previous report [37]. The voltage of the previously reported work is approximately 3.2 V, three times the voltage of our device [38]. The MoO_3 device switching performance has improved almost 2.5 times

by doping 5 wt% Ag and 16 times by doping 10 wt% Ag in the MoO_3 device. These results suggest that the switching performance improvement of the device is only due to addition of Ag in the MoO_3 nanomaterials. Further to understand more detailed performance of the device, the electrical conducting mechanism of the device is analyzed and is discussed in the following section.

3.5. Physical transport mechanism

So as to evaluate the suitability of the devices in neuromorphic application, it is important to recognize the exact mechanism of physical transportation and relationship of resistive switching phenomena with transport mechanism in the system. It is generally approved that the migration of oxygen vacancies because of electrochemical reduction and oxidation plays an essential part in formation and breakup process of conducting filament. Besides, the nanomaterials used as insulating dielectric layer and metals as electrodes would also regulate the conductive mechanism of ReRAM devices substantially. Amongst the commonly observed physical transport mechanism, the Poole-Frenkel emission, Schottky emission, space-charge-limited conduction (SCLC), trap-assisted tunneling (TAT) and hopping conduction are identified in the most of the memory resistive switching devices [39].

To investigate the carrier conductance mechanism, the double logarithmic IV curve was analyzed. In low voltage region, the slope of IV curve is \sim 1, and slope increases to more than 2 for high voltage

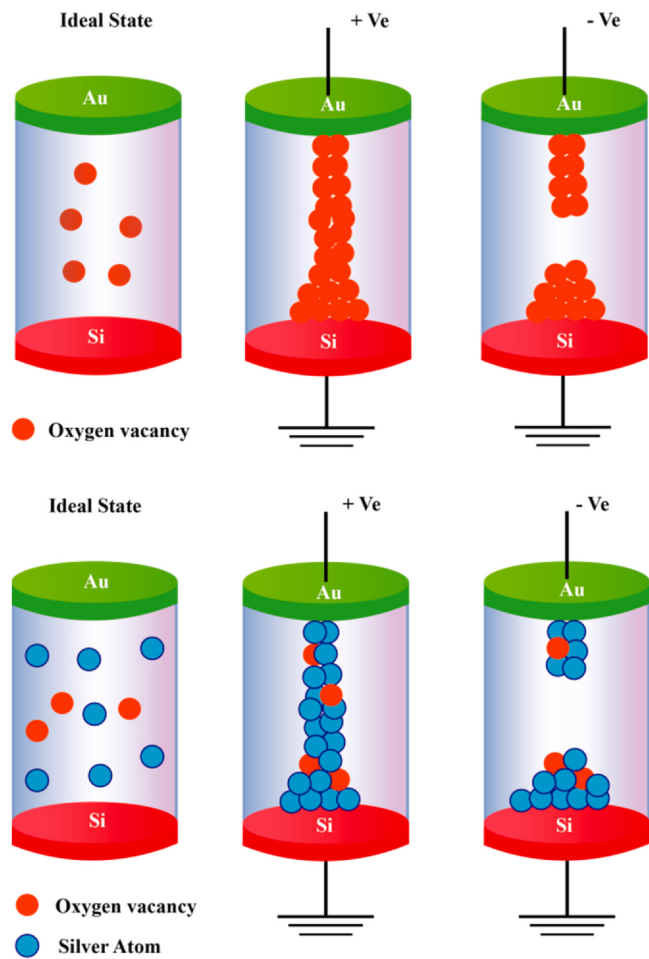


Fig. 9. schematic illustration of the resistive switching mechanism of devices.

region. This confirms the space charge limited conduction current is dominated in the device. The SCLC conduction is expressed as [40],

$$J_{scl} = q^{1-l} \mu N \left(\frac{2l+1}{l+1} \right)^{l+1} \left(\frac{l \epsilon_r \epsilon_0}{l+1 - N_t} \right)^l \frac{V^{l+1}}{d^{2l+1}} \quad (11)$$

Where J represents current density, q represents charge of the element, l represents ratio of temperature difference between characteristics and operation, μ represents the mobility of the charge carriers, N represents density of states, ϵ_r represents permittivity of the active material, ϵ_0 represents free space permittivity, N_t represents trap density, V represents voltage and d represents thickness. When electric field is applied, injected charge carriers fill the defect traps and create more space charge carriers. And thus, the device function under trap filled space charge conduction state.

In the direction of clear understanding the resistive switching mechanism and the charge transport property in the MoO_3 memory clearly, IV characteristics curves are analyzed with double logarithmic scale plot. Fig. 8a-c show the I-V curves of pure MoO_3 and 5 wt% and 10 wt% Ag doped MoO_3 devices for positive bias voltage. For all type of devices, a linear ohmic behavior (slope ~ 1), i.e., linear changes in conductivity with corresponding to applied voltage, is observed in the low-resistance curve of the device. However, the observed curves in high resistive state of all devices are dissimilar to low resistive state curve, which is attributed to the formation of the conducting path in the active material [41,42]. Three distinguished regions are simply recognized in high resistive state of device with various applied voltage. These three-stage variations of conductivity may be contributed to the trap-controlled space charge limited

current (SCLC) mechanism [39]. Accordingly, the SCLC mechanism consists of ohmic region, the Child's law region (slope > 2), and the steep region. In the low bias voltage region, the injected charge carriers, which is greater than thermally induced carriers, will put device in ohmic region of SCLC mechanism. Thus, the density of the free charge carriers is dominated injected ions in the active layer [42,43]. Subsequently, the device will switch to SCLC child law region which applied bias voltage reaches the critical voltage transition region.

The same transition from ohmic to child law region is observed in the all MoO_3 devices. This transition is experimentally detected about 0.5 V in all devices. The slope of child law region of device A, device B and device C are approximately equal to 2.7, 2.3 and 2.5, respectively. In this region, the induced charge carriers will interact with traps available in the nanomaterials and thus conductance mechanism enters into trap filled limited region. Sequentially, space charge appears in the device and sharp increasing current is observed as soon as the applied voltage reaches the trap filled limit. The trap filled limit is observed about ~ 0.8 V for the MoO_3 devices. The similar SCLC characteristic are reported in previous published work for various devices [44,45].

3.6. Conduction switching scheme

The redistribution of native oxygen ions and oxygen vacancies in MoO_3 nanostructure play a critical role in conduction mechanism. Under the electric field, oxygen ions leave their lattice sites and created oxygen vacancies in the switching layer. These results of oxygen ion migration and accumulation in MoO_3 active material is depicted in the figure. When positive voltage is applied on top electrode, the oxygen vacancies accumulate on bottom electrode and oxygen ions migrate to the top electrode. Once the fore most oxygen vacancy filament comes into close vicinity of top electrode, the current rises significantly due to the tunneling process. For instance, the oxygen vacancies are accumulated into vacancy chains. And subsequently, the oxygen deficient nano conducting filament is formed. When negative voltage is applied on top electrode, the oxygen ions move way and accumulate on bottom electrode. Thus, the destruction of conducting path occurs in the structure. Thus, the applied voltage controls the resistance of the active layer in the MoO_3 ReRAM devices. Further, the Ag atoms have been doped in MoO_3 structure to support the ion migration and conductive filament formation. The dopant influenced resistive switching mechanism is also discussed in detail below.

The resistive switching mechanism of fabricated devices is proposed and developed a scheme based on the space charge limited current theory. The schematic representation of device switching mechanism is shown in Fig. 9. The scheme explains the migration of oxygen vacancies and doped silver atoms for the formation of conductive path in the active medium. For undoped device, the conducting path formation is dominated by oxygen vacancies in MoO_3 film. The randomly distributed oxygen vacancies are accumulated and oriented as the positive applied voltage direction. Thus, conduction path by oxygen vacancies modifies the HRS of the device to LRS during SET process. The discontinuity of the conducting path alters the LRS of the device to HRS during negative bias voltage. The conductance change is attributed to the redistribution of oxygen vacancies within the MoO_3 nanomaterial by creating or removing conductive regions between the two electrodes. In Ag doped devices, the Ag atoms also assists the formation of conducting filament along with oxygen vacancies.

When the applied voltage sweeps from 0 V to $+1$ V, Ag atoms were oxidized to Ag^+ cations. But, the oxidation from Ag^+ to Ag_2^+ is not possible in this voltage range as it takes place in higher potential range. Once the applied voltage on top electrode reaches appropriate point, Ag^+ cations drift across the MoO_3 thin film and

travel toward the BE. Additionally, Ag^+ ions are reduced to nonionic Ag atoms and deposited on the BE by electrodeposition process [46] as shown in figure. Subsequently, a conductive path between top and bottom electrodes is created by already deposited silver atoms on the bottom electrode. An adequate negative voltage is applied to top electrode to create disruption in the conducting filament, thus the device switch back again into high resistance state. The Ag^+ cations move toward the top electrode in negative applied voltage and get reduced to Ag atoms. Thus, the HRS state is achieved by annihilating conducting filament by negative voltage. The increased switching resistance ratio in Ag doped MoO_3 device also proposes that Ag doped atoms supports the conducting filament formation in the devices. The reproducibility of such conductive filament is also investigated for Au/Pure $\text{MoO}_3/\text{p-Si}$ and Au/Ag (5 wt% and 10 wt%) doped $\text{MoO}_3/\text{p-Si}$ RRAM devices.

3.7. Operational reliability

The memory performance characteristics like cumulative probability and endurance cycles of the devices were examined to estimate operational reliability. If a memristor loses plasticity after several operations, it is obviously not suitable for neuromorphic application. The cumulative probability will be the suitable analysis to understand the operational uniformity of fabricated memory devices. The cumulative probability distribution of the Au/Pure

$\text{MoO}_3/\text{p-Si}$ and Au/Ag (5 wt% and 10 wt%) doped $\text{MoO}_3/\text{p-Si}$ RRAM device resistance is shown in the figure. The memory units of all devices showed a narrow distribution in both ON and OFF resistive states. The resistive values of the device in HRS and LRS states were statistically examined by applying 50 sweeping cycles. The endurance cycle of all devices is shown in Fig. 10. The good endurance properties of memory devices are experimentally observed in repeated voltage cycles. The undoped MoO_3 device shows small fluctuation in repeated cycles, while more stable repetitive resistance states are observed in silver atom doped MoO_3 devices. The endurance study confirms the reliable switching property of the devices as very less variation of the resistance is observed in the study. The retention characteristics of Au/ $\text{MoO}_3/\text{p-Si}$ and Au/Ag: $\text{MoO}_3/\text{p-Si}$ ReRAM device resistance is depicted in the Fig. 10. The undoped device has less stable retention property while the Ag added device shows improved stable retention properties.

The fluctuation in resistive switching values of undoped device may be due to random nature of formation and annihilation of conducting filaments in the active nanomaterial. The fluctuation in conducting filament formation is resolved by doped silver atoms in the MoO_3 nanomaterials. The addition silver atom suppresses the random nature and stabilize the conductive filaments in active region. The presence of silver ions in the MoO_3 nanostructure create the preferential conductive path dominated by Ag ions and increases the uniformity in conductive path. Thus, doped Ag atom

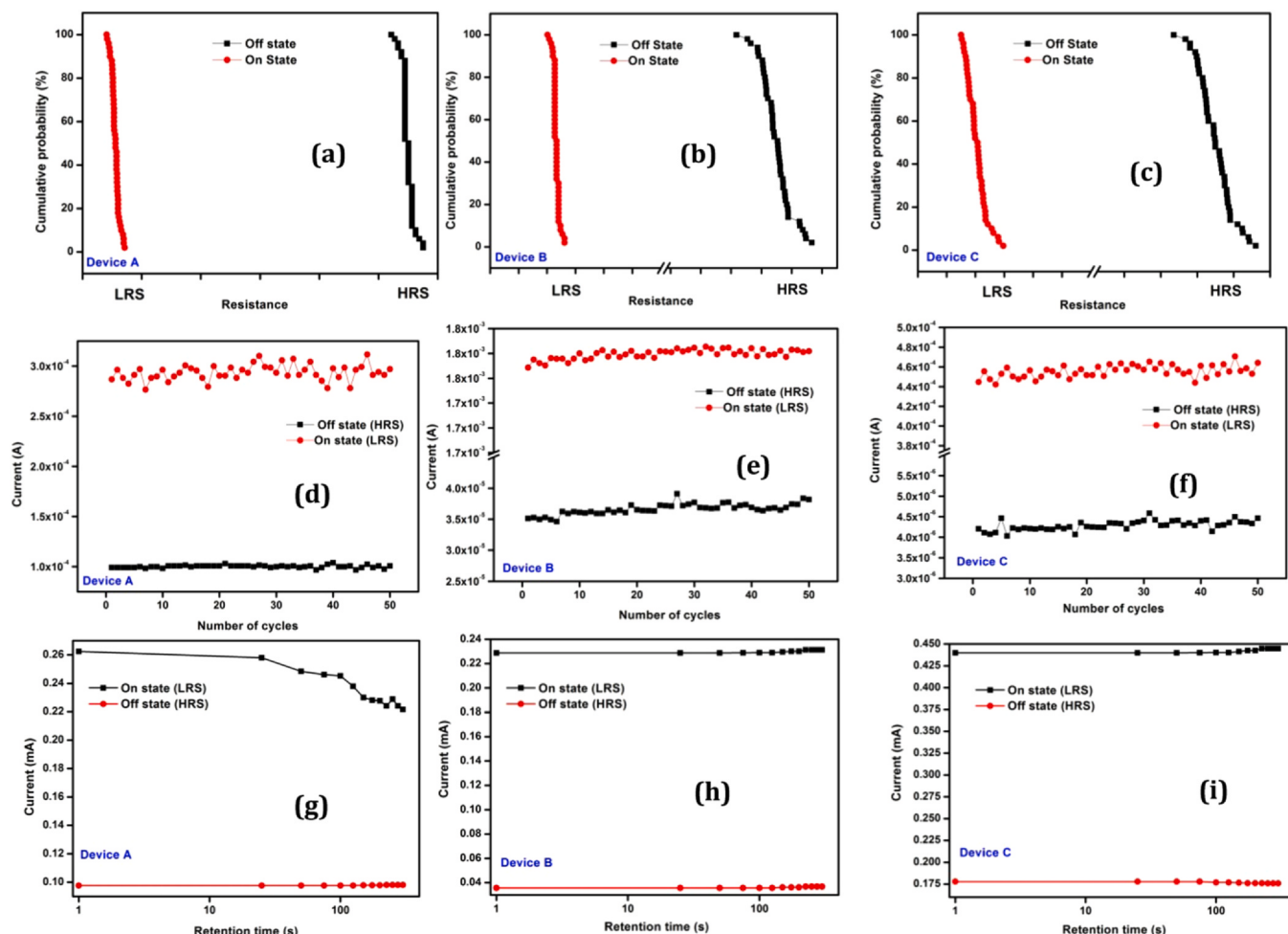


Fig. 10. The cumulative probability (a-c), endurance (d-f) and retention (g-i) analysis of MoO_3 devices: (a) pure MoO_3 (b) 5 wt% of Ag doped MoO_3 (c) 10 wt% of Ag doped MoO_3 probability curve, (d) pure MoO_3 (e) 5 wt% of Ag doped MoO_3 (f) 10 wt% of Ag doped MoO_3 endurance, (g) pure MoO_3 (h) 5 wt% of Ag doped MoO_3 (i) 10 wt% of Ag doped MoO_3 retention study.

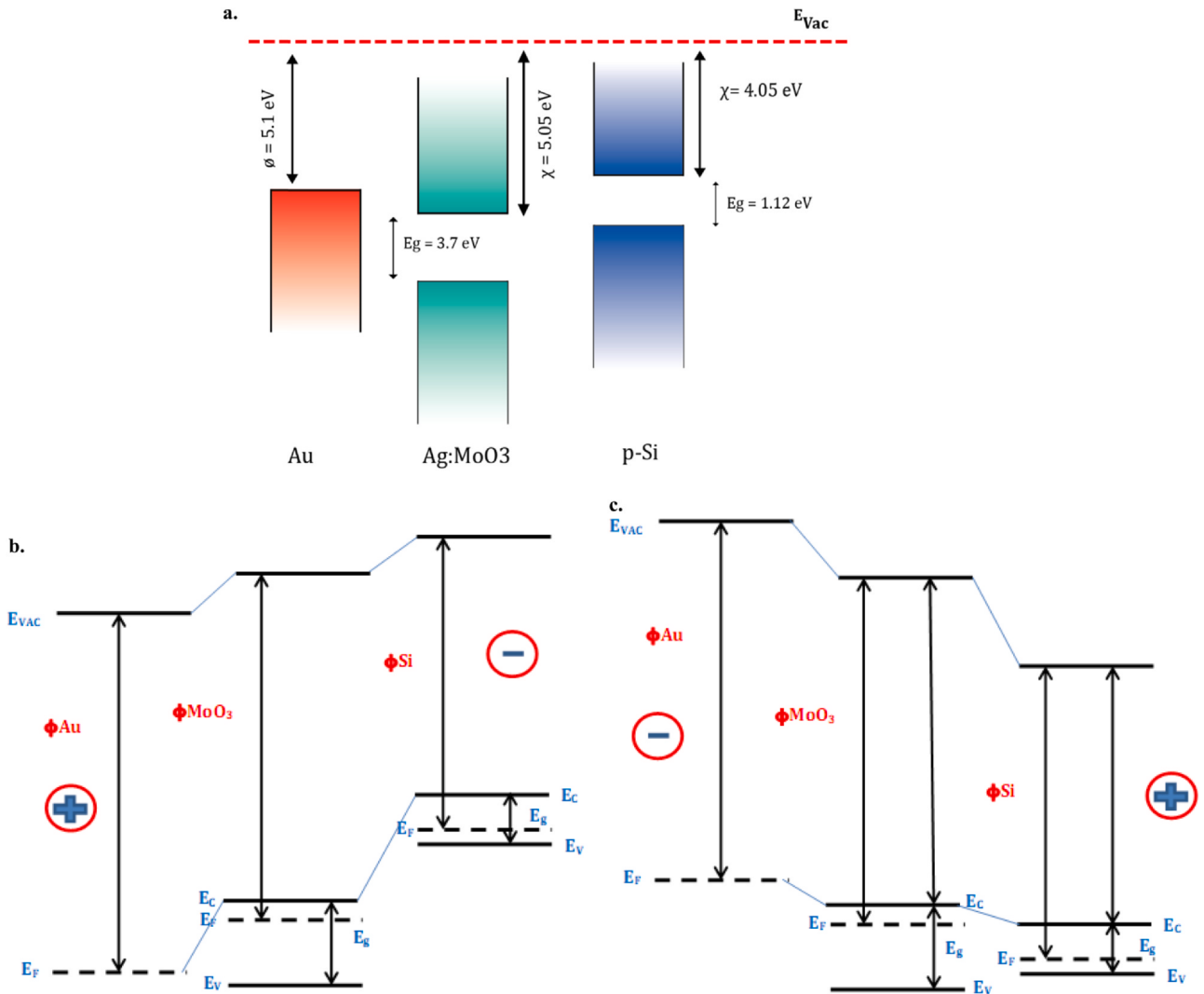


Fig. 11. (a) Energy band diagram of prepared memristor device (b-c) SET and (b) RESET state of Au/ MoO₃/p-Si ReRAM devices.

effectively reduces the randomness in resistive switching mechanism of the devices. Furthermore, increasing the dopant level, the formation and annihilation of the conductive path is more stabilized in additionally silver atoms doped MoO₃ device. It is found that V_{set}, V_{reset}, HRS, and LRS are more uniform when MoO₃ is doped with Ag. Hence, the device added with Ag atom will be more suitable for resistance switching applications than undoped MoO₃ device.

3.8. Energy band analysis

The energy band diagram of the proposed memory device before applying the external bias is presented in Fig. 11a-c. The MoO₃ has high work function value of ~6.7 eV with a high carrier concentration. However, MoO₃ tends to rapidly reduce to MoO_{3-x} during the device fabrication process [46]. Hence, work function is degraded to approximately 5 eV. The reduced MoO_{3-x} gives rise to separated d-d and d-d* gap and thus a smaller density of carriers is available for transport in the material. A disparity in working function value of metal and a semi-conductive nanomaterial is thought to explain the charge injection from the metal through the interface of nanomaterials. The extent of their electron affinity would have contributed to a band alignment between the nanomaterials of MoO₃ and the substrate. Electrons in the interior of the P-Si may flow over the interfacial states, causing the drive belt and the valence belt to bend

upwards. This then forms a lower depletion layer near the device's interface. Consequently, this possible barrier prohibits charge carriers from traveling freely, without any external bias. In addition, the Au electrode and the MoO₃ active layer are formed by ohmic contact.

The direction of diffused electrons is the same as the direction of the ambient electric field applied in the reverse. Only a few load carriers can cross the interface in a small amount of externally applied electric field, and thus the device works in the HRS because the amount of freely moving electrons is smaller. As the applied bias increases, most carriers continue to flow from the electrode into the interface where they are trapped by MoO₃ and due to this sudden increase in electronic drift with increasing voltage, the thickness of the depletion layer decreases. As a result, the effective potential barrier height for charge carriers to cross the interface decreases and hence, the energy band moves downwards. The downward shift in conduction and valence bands has resulted in an increase in the availability of trap sites for charge carriers. Once the effective height of the potential barrier is lowered for free flow carriers, it will be very easy for them to tunnel through the reduced potential barrier. By further increasing the voltage, the potential barrier is finally demolished and the electron injected from the metal electrode can flow freely through the conduction band of the active layer until all the traps are filled. The Ag doped atoms further reduce the potential barrier and promote the formation of the conduction band in the device [47].

These changes of the potential barrier bring the device to the LRS where the data can be stored or written easily. When the bias of the applied voltage is reversed, the trapped electrons from the inside of the MoO_3 and the p-Si gain enough energy to return to the Au electrode. This effective removal of carrier sites results in the device being returned to its original HRS resistance. This trapping and detachment of the charging carriers is well supported by the double I – V logarithmic curves as shown in Fig. 6. The I – V curves indicate that the conduction mechanism is due to space charge limited current (SCLC) model. As a result, the width of the potential barrier will again begin to increase. This makes clear that it is easy to remove the stored data by reverting the polarity of the applied voltage to a rewrite data in the device.

4. Conclusion

The MoO_3 and Ag doped MoO_3 nanoparticles have been successfully synthesized via a wet chemical route. The XRD analysis confirms the formation of pure and Ag doped MoO_3 nanostructures. The morphology of the synthesized nanorods was analyzed by SEM and TEM. HRTEM images revealed that monocrystalline nature of the MoO_3 nanoparticles. The presence of Ag atom in MoO_3 nanostructures was confirmed by these structural studies. In addition, pure MoO_3 (Device A), Ag (5 wt%) doped MoO_3 (Device B), and Ag (10 wt%) doped MoO_3 (Device C) have been fabricated and examined their resistance switching behavior for memristor applications. The ReRAM device results suggest that the resistance ON/OFF performance improvement of the device is only due to addition of Ag in the MoO_3 nanomaterials. The proposed device conduction mechanism was discussed with the help of space charge limited conduction theory. The performance characteristics like cumulative probability and endurance cycles of $\text{Au}/\text{MoO}_3/\text{p-Si}$ and $\text{Au}/\text{Ag}/\text{MoO}_3/\text{p-Si}$ RRAM devices was analyzed and compared for understanding the device mechanism. The results confirmed that the enhanced resistance switching property of Ag doped $\text{Au}/\text{MoO}_3/\text{p-Si}$ device was contributed to Ag doping effect in the formation of conducting filament in the device. Besides, this work anticipated significant information to understand the conducting mechanism to optimize ReRAM devices. Considering the enhanced device characteristics, the silver atoms doped MoO_3 devices may be suitable for nonvolatile random-access memory applications.

Availability of data and materials

The datasets used and/or analyzed during the current study are available from the corresponding author on reasonable request.

Funding

Not Applicable.

CRedit authorship contribution statement

Mohanbabu Bharathi: Conceptualization, Investigation, Writing - original draft. **Babu Balraj:** Writing - review & editing. **Chandrasekar Sivakumar:** Writing - review & editing. **Zhiwei Wang:** Investigation, Drawing. **Jianwei Shuai:** Supervision. **Mon-Shu Ho:** Supervision, Writing - review & editing. **Donghui Guo:** Supervision, Writing - review & editing.

Declaration of Competing Interest

The authors declare that they have no known competing financial interests or personal relationships that could have appeared to influence the work reported in this paper.

Acknowledgments

This work is supported by the Key project's funding of NSFC (No.61836010) and the fundings of National Key Research and Development Program of China (No.2019YFB2204600, No.2019YFB2205001 and No. 2019YFB2205005). This work is also supported by the National Natural Science Foundation of China with Grant Nos. 11874310 and 11675134.

References

- [1] E.M. Vogel, Technology and metrology of new electronic materials and devices, *Nat. Nanotechnol.* 2 (2007) 25–32.
- [2] Q. Xia, J.J. Yang, Memristive crossbar arrays for brain-inspired computing, *Nat. Mater.* 18 (2019) 309–323.
- [3] L. Chua, Memristor—the missing circuit element, *IEEE Trans. Circuit Theory* 18 (1971) 507–519.
- [4] D.B. Strukov, G.S. Snider, D.R. Stewart, R.S. Williams, The missing memristor found, *Nature* 453 (2008) 80–83.
- [5] R. Waser, M. Aono, Nanoionics-based resistive switching memories, *Nat. Mater.* 6 (2007) 833–840.
- [6] R. Waser, R. Dittmann, G. Staikov, K. Szot, Redox-based resistive switching memories – nanoionic mechanisms, prospects, and challenges, *Adv. Mater.* 21 (2009) 2632–2663.
- [7] Y. Yang, W. Lu, Nanoscale resistive switching devices: mechanisms and modeling, *Nanoscale* 5 (2013) 10076–10092.
- [8] L. Goux, I. Valov, Electrochemical processes and device improvement in conductive bridge RAM cells, *Phys. Stat. Solidi A* 213 (2016) 274–288.
- [9] Lei Zhang, Tian Gong, Huide Wang, Zhinan Guo, Han Zhang, Memristive devices based on emerging two-dimensional materials beyond graphene, *Nanoscale* 11 (2019) 12413–12435.
- [10] F. Pan, S. Gao, C. Chen, C. Song, F. Zeng, Recent progress in resistive random access memories: materials, switching mechanisms, and performance, *Mater. Sci. Eng. R* 83 (2014) 1–59.
- [11] C. Gu, J.S. Lee, Flexible hybrid organic-inorganic perovskite memory, *ACS Nano* 10 (2016) 5413–5418.
- [12] N. Onofrio, D. Guzman, A. Strachan, Atomic origin of ultrafast resistance switching in nanoscale electrometallization cells, *Nat. Mater.* 14 (2015) 440–446.
- [13] Z. Wang, S. Joshi, S. Savel'ev, H. Jiang, R. Midya, P. Lin, M. Hu, N. Ge, J. Strachan, Z. Li, Q. Wu, M. Barnell, G. Li, H. Xin, R. Williams, Q. Xia, J. Yang, Memristors with diffusive dynamics as synaptic emulators for neuromorphic computing, *Nat. Mater.* 16 (2016) 101–108.
- [14] Y. van de Burgt, A. Melianas, S.T. Keene, G. Malliaras, A. Salleo, Organic electronics for neuromorphic computing, *Nat. Electron.* 1 (2018) 386–397.
- [15] P. Chi, S. Li, C. Xu, T. Zhang, J. Zhao, Y. Liu, Y. Wang, Y. Xie, PRIME: a novel processing-in-memory architecture for neural network computation in ReRAM-based main memory, in: Proceedings of the 43rd Annual International Symposium on Computer Architecture, 27, (2016).
- [16] T. Hasegawa, K. Terabe, T. Tsuruoka, M. Aono, Atomic switch: atom/ion movement controlled devices for beyond von-neumann computers, *Adv. Mater.* 24 (2012) 252–267.
- [17] K. Qian, G. Cai, V.C. Nguyen, T. Chen, P.S. Lee, Direct observation of conducting filaments in tungsten oxide based transparent resistive switching memory, *ACS Appl. Mater. Interfaces* 8 (2016) 27885–27891.
- [18] A. Khat, S. Cortese, A. Serb, T. Prodromakis, Resistive switching of $\text{Pt}/\text{TiO}_x/\text{Pt}$ devices fabricated on flexible Parylene-C substrates, *Nanotechnol.* 28 (2017) 025303.
- [19] H. Li, Y. Chen, X. Wu, J. Xi, Y. Huang, Z. Ji, Studies on structural and resistive switching properties of $\text{Al}/\text{ZnO}/\text{Al}$ structured resistive random access memory, *Surf. Rev. Lett.* 24 (2017) 1750048.
- [20] H. Jiang, L. Han, P. Lin, Z. Wang, M.H. Jang, Q. Wu, M. Barnell, J.J. Yang, H.L. Xin, Q. Xia, Sub-10 nm Ta channel responsible for superior performance of a HfO_2 memristor, *Sci. Rep.* 6 (2016) 28525.
- [21] J.M. Pachlhofer, C. Jachs, R. Franz, E. Franzke, H. Kostenbauer, J. Winkler, C. Mitterer, Structure evolution in reactively sputtered molybdenum oxide thin films, *Vacuum* 131 (2016) 246–251.
- [22] M.M.Y.A. Alsaif, A.F. Chrimis, T. Daeneke, S. Balendhran, D.O. Bellisario, Y. Son, M.R. Field, W. Zhang, H. Nili, E.P. Nguyen, K. Latham, J. van Embden, M.S. Strano, J.Z. Ou, K. Kalantar-zadeh, High-performance field effect transistors using electronic inks of 2D molybdenum oxide nanoflakes, *Adv. Funct. Mater.* 26 (2016) 91–100.
- [23] T.J. Dai, L.X. Qian, Y.X. Ren, X.Z. Liu, 2017 International Conference on Electron Devices and Solid-State Circuits (EDSSC), 18–20 Oct., (2017).
- [24] M. Janousch, G. Meijer, U. Staub, B. Delley, S. Karg, B. Andreasson, Role of oxygen vacancies in Cr-doped SrTiO_3 for resistance-change memory, *Adv. Mater.* 19 (2007) 2232–2235.
- [25] M. Arita, H. Kaji, T. Fujii, Y. Takahashi, Resistance switching properties of molybdenum oxide films, *Thin Solid Films* 520 (2012) 4762–4767.
- [26] Masashi Arita, Yuuki Ohno, Yosuke Murakami, Keisuke Takamizawa, Atsushi Tsurumaki-Fukuchi, Yasuo Takahashi, *Nanoscale* 8 (2016) 14754–14766.
- [27] H. Zhang, B. Gao, B. Sun, G. Chen, L. Zeng, L. Liu, X. Liu, J. Lu, R. Han, J. Kang, B. Yu, Ionic doping effect in ZrO_2 resistive switching memory, *Appl. Phys. Lett.* 96 (2010) 123502.
- [28] X.W. Jiang, G.Z. Dai, S.B. Lu, J.Y. Wang, Y.H. Dai, J.N. Chen, Wuli Xuebao, *Acta Physica Sinica* 64 (2015) 09130.

- [29] S. Goswami, A.J. Matula, S.P. Rath, S. Hedström, S. Saha, M. Annamalai, D. Sengupta, A. Patra, S. Ghosh, H. Jani, S. Sarkar, M.R. Motapothula, C.A. Nijhuis, J. Martin, S. Goswami, V.S. Batista, T. Venkatesan, Robust resistive memory devices using solution-processable metal-coordinated azo aromatics transducers, *Nat. Mater.* 16 (2017) 1216–1224.
- [30] Lei Wu, Hongxian Liu, Jiabin Li, Shulong Wang, Xing Wang, A multi-level memristor based on Al-doped HfO_2 thin film, *Nanoscale Res. Lett.* 14 (2019) 177.
- [31] Z. Wang, S. Joshi, S.E. Savel'ev, H. Jiang, R. Midya, P. Lin, M. Hu, N. Ge, J.P. Strachan, Z. Li, Q. Wu, M. Barnell, G. Li, H.L. Xin, R.S. Williams, Q. Xia, J.J. Yang, Memristors with diffusive dynamics as synaptic emulators for neuromorphic computing, *Nat. Mater.* 16 (2017) 101–108.
- [32] F.A. Kroeger, H.J. Vink, Relations between the concentrations of imperfections in solids, *J. Phys. Chem. Solids* 5 (1958) 208–223.
- [33] Naseem Bate, Hongfei Shi, Li Chen, Jiabo Wang, Shasha Xu, Weilin Chen, Jianping Li, Enbo Wang, Micelle-directing synthesis of Ag-doped WO_3 and MoO_3 composites for photocatalytic water oxidation and organic-dye adsorption, *Chem. Asian J.* 12 (2017) 2597–2603.
- [34] B. Jansi Rani, G. Ravi, R. Yuvakkumar, F. Ameen, S. Al Nadhari, S.I. Hong, Fabrication and electrochemical OER activity of Ag doped MoO_3 nanorods, *Mater. Sci. Semicond. Process.* 107 (2020) 104818.
- [35] M. Sajadi, M. Ranjbar, R. Rasuli, Two-step synthesis of Ag-decorated MoO_3 nanotubes, and the effect of hydrogen doping, *Appl. Surf. Sci.* 527 (2020) 146675.
- [36] K. Jung, Y. Kim, W. Jung, H. Im, B. Park, J. Hong, J. Lee, J. Park, J.-K. Lee, Electrically induced conducting nanochannels in an amorphous resistive switching niobium oxide film, *Appl. Phys. Lett.* 97 (2010) 233509.
- [37] J. Fatheema, T. Shahid, M. Mohammad, A. Islam, F. Malik, D. Akinwande, S. Rizwan, A comprehensive investigation of MoO_3 based resistive random access memory, *RSC Adv.* 10 (33) (2020) 19345.
- [38] Fahmida Rahman, Taimur Ahmed, a Sumeet Walia, Edwin Mayes, Sharath Sriram, Madhu Bhaskaran, Sivacarendran Balendhran, Reversible resistive switching behaviour in CVD grown, large area MoO_x , *Nanoscale* 42 (2018) 19711.
- [39] Ee. Wah Lim, Razali Ismail, Conduction mechanism of valence change resistive switching memory: a survey, *Electronics* 4 (2015) 586–613.
- [40] J.M. Luo, S.H. Chen, S.L. Bu, J.P. Wen, Resistive switching and Schottky diode-like behaviors in $\text{Pt}/\text{BiFeO}_3/\text{ITO}$ devices, *J. Alloy Compd.* 601 (2014) 100–103.
- [41] U. Celano, Y. Yin Chen, D. Wouters, G. Groeseneken, M. Jurczak, W. Vandervorst, Filament observation in metal-oxide resistive switching devices, *Appl. Phys. Lett.* 102 (2013) 121602.
- [42] J.Y. Chen, C.L. Hsin, C.W. Huang, C. Chiu, Y. Huang, S. Lin, W. Wu, L. Chen, Dynamic evolution of conducting nanofilament in resistive switching memories, *Nano Lett.* 13 (2013) 3671–3677.
- [43] R.W.I. De Boer, A.F. Morpurgo, Influence of surface traps on space-charge limited current, *Phys. Rev. B* 72 (2005) 073207.
- [44] S.Y. Wang, C.W. Huang, D.Y. Lee, T.Y. Tseng, T.C. Chang, Multilevel resistive switching in $\text{Ti}/\text{Cu}_x\text{O}/\text{Pt}$ memory devices, *J. Appl. Phys.* 108 (2010) 114110.
- [45] S. Kim, H.Y. Jeong, S.Y. Choi, Y.K. Choi, Comprehensive modeling of resistive switching in the $\text{Al}/\text{TiO}_x/\text{TiO}_2/\text{Al}$ heterostructure based on space-charge-limited conduction, *Appl. Phys. Lett.* 97 (2010) 033508.
- [46] I. Valov, R. Waser, J.R. Jameson, M.N. Kozicki, Electrochemical metallization memories—fundamentals, applications prospects, *Nanotechnology* 22 (2011) 254003.
- [47] Z. Yin, M. Tordjman, Y. Lee, A. Vardi, R. Kalish, J. del Alamo, Enhanced transport in transistor by tuning transition-metal oxide electronic states interfaced with diamond, *Sci. Adv.* 4 (2018) eaau0480.